

# Does confining the hard-sphere fluid between hard walls change its average properties?

Jeetain Mittal<sup>a)</sup>

*Department of Chemical Engineering, The University of Texas at Austin, Austin, Texas 78712*

Jeffrey R. Errington<sup>b)</sup>

*Department of Chemical and Biological Engineering, University at Buffalo, The State University of New York, Buffalo, New York 14260*

Thomas M. Truskett<sup>c)</sup>

*Department of Chemical Engineering and Institute for Theoretical Chemistry, The University of Texas at Austin, Austin, Texas 78712*

(Received 23 April 2007; accepted 16 May 2007; published online 27 June 2007)

We use grand canonical transition-matrix Monte Carlo and discontinuous molecular dynamics simulations to generate precise thermodynamic and kinetic data for the equilibrium hard-sphere fluid confined between smooth hard walls. These simulations show that the pronounced inhomogeneous structuring of the fluid normal to the confining walls, often the primary focus of density functional theory studies, has a negligible effect on many of its average properties over a surprisingly broad range of conditions. We present one consequence of this insensitivity to confinement: a simple analytical equation relating the average density of the confined fluid to that of the bulk fluid with equal activity. Nontrivial implications of confinement for average fluid properties do emerge in this system, but only when the fluid is *both* (i) dense *and* (ii) confined to a gap smaller than approximately three particle diameters. For this limited set of conditions, we find that “in-phase” oscillatory deviations in excess entropy and self-diffusivity (relative to the behavior of the bulk fluid at the same average density) occur as a function of gap size. These paired thermodynamic/kinetic deviations from bulk behavior appear to reflect the geometric packing frustration that arises when the confined space cannot naturally accommodate an integer number of particle layers. © 2007 American Institute of Physics. [DOI: [10.1063/1.2748045](https://doi.org/10.1063/1.2748045)]

## I. INTRODUCTION

Confined fluids play an important role in a host of scientific phenomena and technological applications. Examples range from the aqueous fluids that fill the cytostructures of biological cells to the solvents that facilitate the operation of nano- and microfluidic devices, membranes for separations, and porous catalytic materials. In many of these systems, confinement significantly modifies the thermodynamic and kinetic behavior of the fluid relative to the bulk phase. Such modifications are generally attributed to the collective effects of the size and shape of the confined space and the interactions of the fluid with the confining surfaces. However, isolating the individual contributions of these various factors for study can be a daunting experimental task.

Given this difficulty, one alternative approach has been to explore the behavior of simplified models that allow one to examine the implications of confinement in the absence of the complicating details that are present in experimental systems. Along these lines, a commonly investigated model is the equilibrium, monatomic hard-sphere (HS) fluid confined between smooth and parallel hard walls. This is arguably the most basic model that can capture the main entropic packing

effects associated with fluids in confined spaces. Its characteristic inhomogeneous density profile (normal to the confining walls), which has been a primary focus of previous investigations, is now qualitatively understood.<sup>1</sup> Unfortunately, despite progress in elucidating some of the other properties of this system,<sup>1–11</sup> a comprehensive picture for precisely how confinement modifies the average thermodynamic and kinetic behavior of the equilibrium HS fluid has yet to emerge.

One of the most basic hurdles in constructing this picture has been the lack of accurate molecular simulation data for the average properties of the confined HS fluid, a fact that may seem surprising given the apparent simplicity of the model. Ironically, the model’s simplicity has indirectly contributed to the lack of simulation data because it has allowed the system to be readily studied by approximate theories instead,<sup>12,13</sup> which are appealing because they are physically insightful and require only modest computational resources. However, the development of efficient algorithms for investigating systems with discontinuous potentials and the availability of fast computers have now made it feasible to use molecular simulation to fully characterize the behavior of this model with both accuracy and precision. One aim of the present study is to leverage these simulation resources to take an important step toward completing this characterization.

The data that we present here provide some insights into

<sup>a)</sup>Electronic mail: jeetain@che.utexas.edu

<sup>b)</sup>Electronic mail: jerring@buffalo.edu

<sup>c)</sup>Electronic mail: truskett@utexas.edu

an important, but still poorly understood, conceptual point concerning this model. Specifically, it has not been entirely clear how one should compare the confined fluid to the bulk fluid in order to elucidate the main effects of confinement. One obvious possibility is to compare the two systems under conditions where they exhibit equal “average” density. The argument for choosing this basis of comparison is straightforward. Packing effects dominate the behavior of athermal systems, and average density is an important factor in determining how the particles pack. Moreover, if one controls for average density in making the comparison, then one can hope to isolate more subtle effects due to, e.g., the finite size of the confined system (in one direction) and the shape of the density profile (i.e., the “layering”). Another possibility is to compare the two systems at equal activity, where the bulk and pore fluids exhibit different average densities. The advantage in doing so is also obvious. Equality of activity is a relevant experimental constraint on the chemical equilibrium that is established between the bulk and pore fluids.

The complication in comparing the two systems at the same density is that there are two different definitions for average density that are commonly invoked:  $\rho = N\sigma^3/V$  and  $\rho_h = N\sigma^3/V_h$ . Here,  $N$  refers to the number of particles and  $\sigma$  is the particle diameter. The difference between the two is that  $V = AH$  is the total volume of the confined fluid (i.e.,  $A$  is the area of a wall in contact with the fluid, and  $H$  is the distance from “wall surface to wall surface”), while  $V_h = Ah$  is the smaller volume accessible to the particle centers (i.e.,  $h = H - \sigma$ ). While densities based on these two definitions converge in the limit  $H \rightarrow \infty$ , they can be quite different for severely confined fluids. We are not aware of any systematic comparisons of how the thermodynamic properties of this system depend on  $\rho$  and  $\rho_h$ , respectively.

However, even in the absence of such comparative studies, it is easy to imagine that one might indeed arrive at qualitatively different conclusions about the implications of confinement depending on whether  $\rho$  or  $\rho_h$  is chosen as the basis for comparison. To appreciate this point, consider that  $\rho_h$  diverges in the limit where the gap size  $H$  is reduced, at fixed  $N/A$ , to the size of one particle diameter  $\sigma$  (i.e., the two-dimensional fluid limit), whereas  $\rho$  and many other fluid properties of interest remain finite. This type of consideration alone hints that  $\rho$  might be the more suitable density variable of the two for making comparisons to the bulk fluid, and indeed  $\rho$  naturally emerges in the thermodynamic analysis of confined HS fluids.<sup>5,6</sup>

More concrete evidence supporting the use of  $\rho$  rather than  $\rho_h$  for comparing confined and bulk fluids comes from studies of transport properties. Specifically, it has recently been demonstrated via molecular simulation<sup>7</sup> that the self-diffusivity of the confined HS fluid parallel to the confining walls, over a broad range of equilibrium conditions, is very similar to the diffusion coefficient of the bulk HS fluid if the two systems are compared at the same value of  $\rho$ . In other words, the specific details of the inhomogeneous packing structures have only minor influence on the average single-particle dynamics of the confined fluid, as long as one controls for the average overall density  $\rho$ . Alternatively, if one

instead compares the behaviors of the bulk and confined systems at equal values of  $\rho_h$ , one arrives at the conclusion that confining a HS fluid between hard walls has the effect of significantly speeding up its dynamics. This latter artificial conclusion is related to the fact that  $N/A$  must vanish if  $\rho_h$  is to remain constant in the limit  $H \rightarrow \sigma$ . As a result, even if the numerical value of  $\rho_h$  is chosen to be indicative of a dense bulk fluid, the actual average interparticle separation and particle mobility in the lateral direction will generally be very large (e.g., comparable to a dilute gas) when the fluid is confined to small enough  $H$ .

In this paper, we follow up on some of these initial observations by presenting a more comprehensive study of how fluid density and confinement (between hard walls) affect the thermodynamic and kinetic properties of the HS fluid. We broadly focus our investigation on four main questions. The first pertains to the equation of state of the confined fluid (i.e., how the average transverse and normal components of its pressure tensor vary with average density). Specifically, we are interested in how the behaviors of these pressure components depend on the volume definition invoked, i.e.,  $V$  vs  $V_h$ . Does the use of either definition produce relationships similar to the equation of state of the bulk HS fluid? Second, what are the effects of confinement and average density on the transverse self-diffusivity of fluids confined to pores narrower than those previously examined<sup>7</sup> (i.e.,  $H < 3.5\sigma$ )? Third, how do the behaviors of the confined and bulk HS fluid systems compare under conditions of equal activity as opposed to equal density? Finally, does the robust relationship between excess entropy  $s^{\text{ex}}$  (relative to ideal gas) and self-diffusivity  $D$ , previously discovered for fluids confined to gap sizes larger than  $H = 3.5\sigma$  in this system,<sup>7</sup> continue to hold for very narrow pores ( $H < 3.5\sigma$ )? By addressing these four questions, we can make significant headway not only in identifying the regions in the  $H$ - $\rho$  and  $H$ - $\xi$  planes of parameter space where the confined HS system significantly deviates from the bulk HS fluid, but also in probing the microscopic mechanisms for such deviations.

## II. SIMULATION METHODS

To explore these issues, we have calculated the thermodynamic properties of confined and bulk HS fluids using grand canonical transition-matrix Monte Carlo (GC-TMMC) simulations,<sup>14,15</sup> and we have tracked their single-particle dynamics via discontinuous molecular dynamics (DMD) simulations.<sup>16</sup> To simplify the notation in this article, we have implicitly nondimensionalized all quantities by appropriate combinations of a characteristic length scale (which we take to be the HS particle diameter  $\sigma$ ) and time scale (which we choose to be  $\sigma\sqrt{m\beta}$ , where  $m$  is particle mass,  $\beta = [k_B T]^{-1}$ ,  $k_B$  is the Boltzmann constant, and  $T$  is temperature). As a result, all quantities with dimensions of energy are understood to be “per  $k_B T$ ,” the only energy scale in the problem.

The DMD simulations each involved  $N = 1500$  identical HS particles. For the bulk fluid, the particle centers were contained within a cubic simulation cell of  $V_h = N/\rho_h$ ,

and periodic boundary conditions were applied in all three directions. For the confined fluid, particle centers were contained within a rectangular parallelepiped simulation cell of  $V_h = h_x h_y h_z$ , where  $h_z = H - 1$  and  $h_x = h_y = [N / (h_z \rho_h)]^{1/2}$ . Periodic boundary conditions were applied in the  $x$  and  $y$  directions and perfectly reflecting, smooth hard walls were placed so that particle centers were trapped in the region  $0 < z < h_z$ . The self-diffusivity  $D$  of the fluid was obtained by fitting the long-time ( $t \gg 1$ ) behavior of the average mean-squared displacement of the particles to the Einstein relation  $\langle \Delta r_d^2 \rangle = 2dDt$ , where  $\Delta r_d^2$  corresponds to the mean-square displacement per particle in the  $d$  periodic directions ( $d=2,3$  for the confined and bulk fluid, respectively). To verify that system-size effects in the periodic directions on  $D$  were insignificant, we checked if our calculated values for  $D$  for several state points compared favorably with those we obtained using either  $N=3000$  or  $N=4500$  particles.

The GC-TMMC simulations each utilized a simulation cell of size  $V_h = 1000$ . For the bulk fluid, the cell was cubic with  $h_x = h_y = h_z = 10$ . For the confined fluid, the cell was a rectangular parallelepiped with  $h_z = H - 1$  and  $h_y = h_x = \sqrt{1000/h_z}$ . GC-TMMC simulations require a specified value for the activity  $\xi$  (Ref. 17) (i.e.,  $N$  is allowed to fluctuate), and we set  $\xi=1$  in all cases. The key quantities that we extracted from the simulations were the normalized total particle number probability distribution  $\Pi(N)$  and the  $N$ -specific spatial density distribution  $\rho(N, \mathbf{r})$ , both evaluated over a range of particle numbers spanning from  $N=0$  to  $N=984$ . Thermodynamic properties at other values of activity  $\xi$  were readily obtained via the histogram reweighting technique<sup>18</sup> to shift the original  $\Pi(N)$  distribution to one representative of the particle numbers visited at the selected  $\xi$ . We found that we obtained statistically indistinguishable results for systems with  $V_h=500$ , indicating again that noticeable artifacts associated with system size were not present.

By employing basic arguments from statistical mechanics,<sup>1,19</sup> one can use the equilibrium information from GC-TMMC simulations to compute thermodynamic properties of interest. Specifically, the grand potential  $\Omega$  can be calculated directly from the normalized particle number distribution,<sup>19,20</sup>

$$\Omega = \ln \Pi(0). \quad (1)$$

For the bulk HS fluid, we also have  $V=V_h$ , and thus  $\rho = \sum_N N \Pi(N) / V = \rho_h$ . Moreover, the pressure of the bulk fluid  $P$  is equal to the negative of the grand potential density,  $P = -\Omega / V$ . On the other hand, for the HS fluid confined between hard walls, we have  $V = V_h / (1 - H^{-1})$ , and thus  $\rho = \sum_N N \Pi(N) / V = (1 - H^{-1}) \rho_h$ . In this case, negative grand potential density  $-\Omega / V$  represents an average transverse pressure acting parallel to the confining walls.<sup>21</sup> In the reduced units adopted here, the component of the pressure tensor acting normal to the walls is equal to the local fluid density in contact with a hard wall,  $P_z(N) = \rho(N, z=0.5) = \rho(N, z=H-0.5)$ , a consequence of an exact statistical mechanical sum rule for this system.<sup>22</sup> Finally, the molar excess entropy  $s^{\text{ex}} = S^{\text{ex}} / N$  is determined using the following expression:<sup>7,23</sup>

$$S^{\text{ex}}(N) = \ln[\Pi(N)/\Pi(0)] - N \ln \xi + \ln N! - N \ln N + \int \rho(N, \mathbf{r}) \ln \rho(N, \mathbf{r}) d\mathbf{r}. \quad (2)$$

Below, we describe how the above methods were employed in this study to characterize the behaviors of the confined and bulk HS fluids.

### III. RESULTS AND DISCUSSION

#### A. Volume definition and the equation of state

One of the most practically important and well-understood properties of the bulk, equilibrium HS fluid is its equation of state  $P(\rho)$ , which quantifies how its pressure varies with density. For densities below the freezing transition ( $\rho \lesssim 0.943$ ), this relationship is accurately described by the semiempirical Carnahan-Starling equation  $P(\rho) \approx P_{\text{CS}}(\rho) = \rho(1 + \phi + \phi^2 - \phi^3) / (1 - \phi)^3$ ,<sup>24</sup> where  $\phi = \pi\rho/6$  is the packing fraction of the spheres.

Much less is known about the global behavior of the pressure tensor for the HS fluid confined between smooth hard walls. One obvious question is, do the relationships between the transverse and normal components of the pressure tensor and average density (defined as either  $\rho$  or  $\rho_h$ ) show quantitative similarities to the equation of state of the bulk fluid? Although the inhomogeneous structuring of the fluid might be expected to give rise to some nontrivial deviations from bulk fluid behavior, the main qualitative trends should be the same: compressing the fluid increases the interparticle collision rate and, consequently, the individual components of the pressure tensor.

In Fig. 1, we compare the bulk fluid equation of state to our GC-TMMC simulation data for the average transverse and normal components of the pressure tensor. We focus here on confined fluids with  $H=3.5, 6, 8.5,$  and  $16$ . In top panels (a) and (b), negative grand potential density is plotted versus average density, adopting the  $V_h$  (center accessible) and  $V$  (total) volume conventions, respectively. The density dependencies of  $P_z$  are similarly displayed in panels (c) and (d). Focusing on plots (a) and (c), one finds a family of curves for  $-\Omega/V_h$  and  $P_z$  that are qualitatively similar to the bulk fluid behavior, with the main difference being that systems with smaller  $H$  have weaker  $\rho_h$  dependencies (higher apparent compressibilities). This difference appears logically consistent with the earlier observation<sup>7</sup> that confined HS fluids also have faster single-particle dynamics as compared to the corresponding bulk fluid with the same  $\rho_h$ .

Interestingly, the corresponding quantities plotted in (b) and (d) using the total volume  $V$  convention approximately collapse onto a single curve. This means that the  $\rho$  dependencies of both  $-\Omega/V$  and  $P_z$ , for each value of  $H$  investigated, can approximately be described by the equation of state of the bulk fluid  $P(\rho)$ . This trend also appears consistent with the approximate collapse of self-diffusivities for confined HS fluids onto the bulk behavior when plotted together on a single graph versus  $\rho$ .<sup>7</sup> Although there are clearly some quantitative deviations from bulk behavior for the

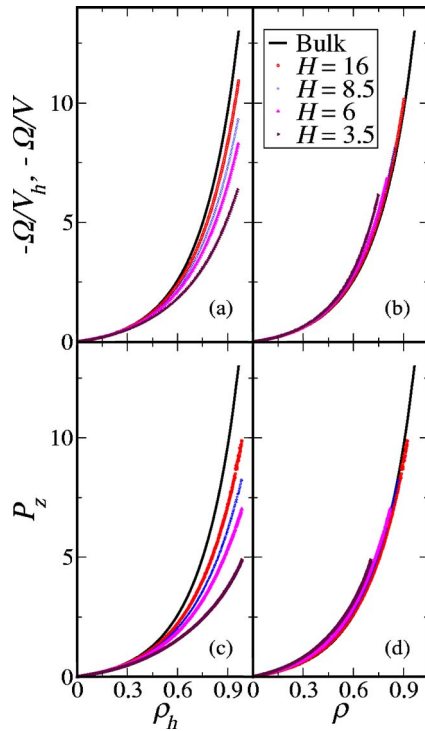


FIG. 1. (Color online) Equation of state of a confined HS fluid between hard walls separated by center-accessible distance  $H-1$ . Top panels show the negative of the grand potential density (average transverse pressure) versus average fluid density calculated using (a) the center-accessible volume  $V_h$  and (b) the total volume  $V$ . Bottom panels illustrate the normal pressure versus average density calculated using (c) the center-accessible volume  $V_h$  and (d) the total volume  $V$ .

smallest pores in panels (b) and (d) of Fig. 1, we found that the following simple relationship can describe the  $\rho$  dependence of the grand potential density to within at least 25% for  $H \geq 3.5$ :

$$\Omega(\rho, H)/V \approx -P_{CS}(\rho). \quad (3)$$

We will use this approximate relationship below to help construct an analytical model for predicting the excess adsorption of fluid in a model slit pore.

## B. Interfacial free energy and excess adsorption

Given the approximate collapse of the thermodynamic data for the confined HS fluid when plotted against average density  $\rho$ , it is natural to ask whether there is a connection to the behavior of the interfacial free energy and the surface excess adsorption of the fluid at a single hard wall.

The interfacial free energy of the HS fluid near a hard wall is defined as the excess grand potential of the fluid (relative to bulk) per unit fluid-wall contact area. Similar to average density, its numerical value depends on the arbitrary choice of dividing surface,<sup>25,26</sup> although different choices provide equivalent thermodynamic descriptions of the system if applied self-consistently. If one chooses the plane of closest approach of the particle centers to the wall as the dividing surface, then the following expression yields the interfacial free energy:

$$\gamma_h^\infty = \lim_{H \rightarrow \infty} \left[ \frac{\Omega(\rho, H)}{V_h} + P_b \right] \frac{(H-1)}{2}, \quad (4)$$

where  $P_b$  is the pressure of the bulk fluid in equilibrium with the pore fluid. Stated differently,  $\rho$  of the pore fluid is determined by  $H$  and the requirement that it adopts the same activity  $\xi$  as the bulk HS fluid of pressure  $P_b$ . There is an accurate approximate equation due to Henderson and Plischke<sup>27</sup> for predicting how  $\gamma_h^\infty$  depends on the packing fraction of the bulk fluid  $\phi_b = \pi\rho_b/6$ ,

$$\gamma_h^\infty \approx -\frac{9}{2\pi} \phi_b^2 \frac{[1 + (44/35)\phi_b - (4/5)\phi_b^2]}{(1 - \phi_b)^3}. \quad (5)$$

If one instead chooses the physical surface of the wall to be the dividing surface, then a slightly different equation emerges:

$$\gamma^\infty = \lim_{H \rightarrow \infty} \left[ \frac{\Omega(\rho, H)}{V} + P_b \right] \frac{H}{2} \quad (6)$$

$$= \gamma_h^\infty + P_b/2. \quad (7)$$

Substituting the Carnahan-Starling equation of state for  $P_b$  and Eq. (5) for  $\gamma_h^\infty$  into Eq. (7) results in the following analytical estimate for  $\gamma^\infty$ :

$$\gamma^\infty \approx \frac{3}{\pi} \phi_b \frac{[1 - (1/2)\phi_b - (31/35)\phi_b^2 + (1/5)\phi_b^3]}{(1 - \phi_b)^3}. \quad (8)$$

Given that we have already observed that other properties of the confined HS fluid approximately collapse when plotted versus  $\rho$  (based on total volume  $V$ ), we choose to focus our attention from this point forward on  $\gamma^\infty$ , the interfacial free energy that is also based on  $V$ .

As we demonstrated in the previous section, one can readily determine the quantities on the right-hand side of Eq. (6) for finite values of  $H$  using GC-TMMC simulations. As a result, these simulations might also provide a reasonably accurate means for estimating  $\gamma^\infty$ , assuming that  $H$  can be chosen large enough so that the perturbations to the fluid caused by the two confining walls do not significantly interfere with one another (i.e., so that the so-called “finite-size” or frustration effects of confinement do not occur). Although, it is not clear *a priori* how large  $H$  must be to achieve this, one might reasonably expect that the pore would need to be at least several particle diameters in width.

As a test of this idea, we present in Fig. 2 the values of the quantity  $[\Omega(\rho, H)/V + P_b](H/2)$  calculated from our GC-TMMC simulations for various  $H$  along with the single-wall quantity  $\gamma^\infty$  of Eq. (8), which is the  $H \rightarrow \infty$  limit. All data are plotted as a function of bulk packing fraction  $\phi_b$ . Interestingly, the plot reveals that the simulated curves for  $H \geq 3.5$  all collapse, to within an excellent approximation, onto that for  $\gamma^\infty$ . In other words,

$$\gamma^\infty \approx \left[ \frac{\Omega(\rho, H)}{V} + P_b \right] \frac{H}{2}, \quad (9)$$

independent of  $H$  for  $H \geq 3.5$ . This implies that the single-wall behavior such as  $\gamma^\infty$  can be estimated with great

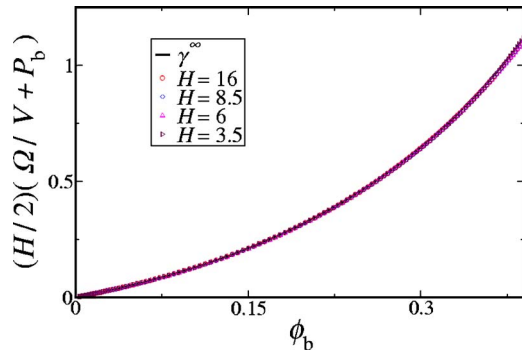


FIG. 2. (Color online) The quantity  $(H/2)[\Omega/V + P_b]$  calculated from our GC-TMMC simulations for various  $H$  along with the  $H \rightarrow \infty$  limit,  $\gamma^\infty$ , computed using Eq. (8). Data are plotted as a function of  $\phi_b$ , the packing fraction of the bulk HS fluid that is in equilibrium with the pore fluid.

accuracy in this system from a simulated slit pore of width  $H=3.5$ , which can only accommodate a fluid film three particle layers thick. This result, while very robust, is somewhat surprising because the single-wall density profiles decay slowly enough to expect appreciable interference or frustration effects at pore sizes as small as  $H=3.5$ . However, similar to the picture that emerged from the behavior of the equation of state in the previous section, any interference that does occur apparently cancels in determining the average properties of the confined HS fluid, which remain remarkably “bulklike” even for these very thin films.

So, when do interference effects due to packing frustration of the wall-induced particle layers begin to occur? We can probe this issue by taking the analysis one step further. Specifically, if one uses Eq. (3) to substitute for  $\Omega(\rho, H)/V$  in Eq. (9), differentiates both sides of Eq. (9) with respect to chemical potential, and invokes the Gibbs adsorption equation  $\partial\gamma^\infty/\partial\mu = -\Gamma^\infty$ , then upon rearranging one arrives at the following simple equation for predicting the pore density  $\rho$ :

$$\rho \approx \rho_b + \frac{2\Gamma^\infty}{H}. \quad (10)$$

The quantity  $\Gamma^\infty$  is the standard surface excess density for a HS fluid next to *single* hard wall, and, within the above approximations, it is given by

$$\Gamma^\infty = -\frac{3\phi_b[1 + a_1\phi_b + a_2\phi_b^2 + a_3\phi_b^3 + a_4\phi_b^4]}{\pi(1 + 4\phi_b + 4\phi_b^2 - 4\phi_b^3 + \phi_b^4)}, \quad (11)$$

where  $a_1=1$ ,  $a_2=-221/70$ ,  $a_3=4/5$ , and  $a_4=-1/5$ .

Figure 3 shows the predictions of the simple analytical model of Eqs. (10) and (11) compared to the simulated pore density  $\rho$  as a function of  $H$ . From the plot, it is evident that the average pore density can be predicted based on knowledge of only the single-wall surface excess  $\Gamma^\infty$  unless the fluid is both dense and confined to pores narrower than approximately three particle diameters. Under those restrictive conditions, the single-wall model misses the emergence of oscillations in the pore density. These oscillations cannot be solely attributed to single-wall layering in the density profile because pronounced layering also occurs for dense fluids with  $H \gg 3$ , where the analytical model is still very accurate. Rather, the oscillations must be due to packing frustration

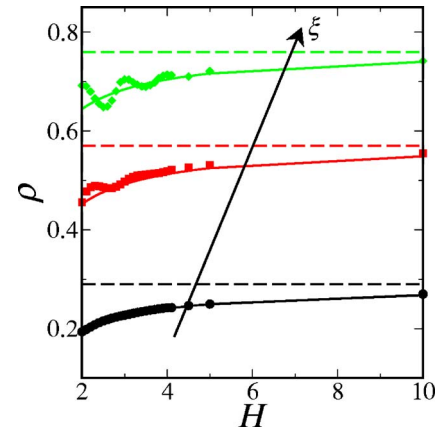


FIG. 3. (Color online) Pore fluid density  $\rho$  as a function of pore width  $H$  at different values of activity [ $\ln \xi = 0.4, 4.4, \text{ and } 8.8$ ]. Filled symbols and solid lines correspond to the GC-TMMC data and the predictions of Eq. (10), respectively. The dashed lines correspond to the bulk density  $\rho_b$  for a given activity  $\xi$ .

associated with the interference of the layers emerging from the two confining walls, which apparently becomes significant in this system only for very narrow pores and high fluid density.

### C. Comparing bulk and pore fluid self-diffusivities

The last two sections demonstrated that some of the average thermodynamic properties of the confined HS fluid are very similar to those of the bulk fluid if the two systems are compared at equal values of the average density  $\rho$  (based on the total system volume). Deviations occur only when the fluid is both dense and confined to pores narrower than approximately three particle diameters. In a previous study,<sup>7</sup> we have also shown that the self-diffusivity  $D$  of the confined HS fluid is approximately equal to that of the bulk fluid with the same  $\rho$  for  $H > 3.5$  over a fairly broad range of  $\rho$ . Here, we carefully investigate the  $H$  dependency of pore self-diffusivity at constant  $\rho$  for narrow pores, with a focus on understanding when packing frustration causes the correlation between  $D$  and  $\rho$  to break down. We also investigate the  $H$  dependency of  $D$  for the confined fluid under the constraint of constant imposed activity  $\xi$ . We find that this latter behavior can be essentially predicted in advance, given the known connection between  $D$  and  $\rho$  (Ref. 7) and the ability to predict  $\rho$  from  $\xi$  and  $H$  discussed in the previous section.

We begin here by examining how  $H$  affects  $D$  at constant  $\rho$  using the DMD simulations described earlier. Specifically, we plot in Fig. 4 the self-diffusivity  $D$  of the bulk and confined HS fluid for  $H=2-5$  and various pore packing fractions ( $\phi \equiv \pi\rho/6 = 0.15, 0.30, 0.40, \text{ and } 0.45$ ). What is plainly evident is that up to fairly dense packing fractions ( $\phi < 0.40$ ), the  $D$  of the confined fluid shows no significant deviations from bulk behavior (dashed line) even when in very restrictive pores (e.g.,  $H=2$ ). In fact, quantitative deviations are prominent ( $>25\%$ ) only in the high density ( $\phi \geq 0.4$ ) and small pore ( $H < 3$ ) limit. Note that an equilibrium fluid at  $\phi=0.45$  cannot be accessed over the full  $H$  range because the system penetrates into the fluid-solid coexistence region or the solid phase region on its phase diagram.<sup>2</sup>

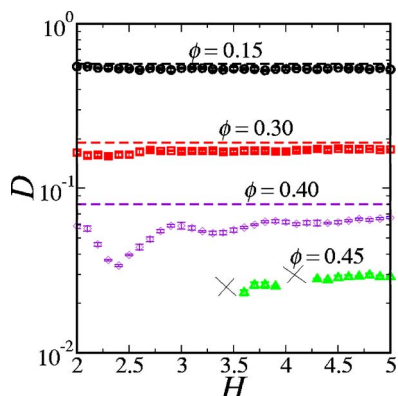


FIG. 4. (Color online) Self-diffusivity  $D$  as a function of pore width  $H$  at different pore fluid packing fractions  $\phi$ . For  $\phi=0.45$ , crosses mark regions for which the confined system penetrates into the fluid-solid coexistence region or the solid phase region on its equilibrium phase diagram. (Ref. 2.)

To gain a more physical understanding of the variations in  $D$  at constant  $\phi$  that occur under conditions of high  $\phi$  and low  $H$ , we plot in Fig. 5 the two-dimensional (2D) projections of instantaneous particle configurations of the confined HS fluid for  $H=2.0$ , 2.4, and 3.0 at  $\phi=0.40$ , state points that show very different dynamical behaviors. We also present the corresponding density profiles  $\rho(z)$  normal to the walls. This figure shows well-developed layering structures for both  $H=2.0$  (two particle layers) and  $H=3.0$  (three particle layers). However, the system at  $H=2.4$  shows considerably more packing frustration. In particular, the individual density peaks are reduced in this case because the spacing is such that it is “in between” distances that naturally accommodate either two or three layers. The pore diffusivity is also lowest for  $\phi=0.4$  at  $H=2.4$  as shown in Fig. 4. Similar oscillations in  $D$ , which are much smaller in magnitude and decay with increasing  $H$ , occur at larger separations with the minima again coinciding with spacings that do not naturally accommodate an integer number of particle layers. In short, for small enough pores and high enough densities, the frustrated layering of particles normal to the confining walls significantly slows down the single-particle dynamics in the direction parallel to the walls.

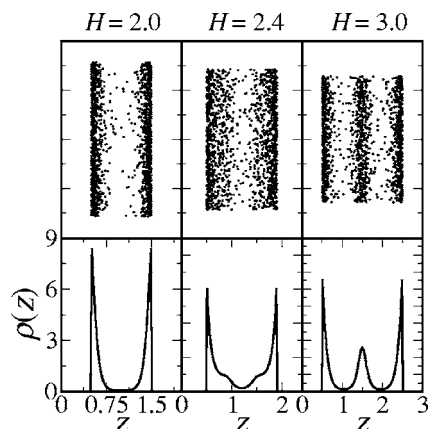


FIG. 5. 2D projections of typical instantaneous particle configurations of the confined HS fluid are shown (top) along with equilibrium density profiles  $\rho(z)$  (bottom), where  $z$  represents the positional coordinate normal to the walls.

The trend that increased layering leads to faster dynamics may initially appear counterintuitive, especially if one tries to understand it by drawing an analogy with the bulk HS system. In the bulk HS system, compressing the fluid increases the structural ordering<sup>28,29</sup> but *reduces* the self-diffusivity. In contrast, as can be clearly seen in Figs. 4 and 5, increased layering in the normal direction (i.e., less uniform density profiles) correlates with faster dynamics. However, these two represent fundamentally different systems undergoing different changes. In the bulk HS system, increasing the density not only increases the structural order, but it also reduces the entropy (or average free volume) of the particles in the fluid. This compression-induced reduction in free volume is not surprisingly correlated with slower dynamics. However, the confined HS system actually maximizes its entropy (or average free volume) at fixed average density and  $H$  by adopting an inhomogeneous density profile with pronounced layering.<sup>30</sup> Our results show that, for constant  $\rho$ , the values of (small)  $H$  that frustrate the ability of the system to form an integral number of particle layers also tend to reduce the single-particle mobility in the direction parallel to the walls. We return to investigate the potential connection between dynamics and entropy of the confined HS fluid in the next section.

Another important point concerning the frustration-induced oscillations in  $D$  of Fig. 4 is that they are distinct from the oscillations in  $D$  that occur as a function of  $H$  at constant activity  $\xi$ .<sup>12,13</sup> The latter are inevitably impacted by oscillations in average pore density, whereas the average density is being controlled for (held constant) in Fig. 4. Deviations from bulk behavior at fixed average density are purely frustration-induced *finite-size effects*, and the relative importance of these types of deviations has been a long-standing question in the study of confined fluids.<sup>31</sup>

Interestingly, if one compares the locations of the oscillations in  $D$  vs  $H$  at  $\phi=0.40$  in Fig. 4 with the fluid-solid phase boundary of this system presented by Fortini and Dijkstra,<sup>2</sup> one also finds a strong correlation between slow dynamics and proximity of the fluid to the phase boundary. In other words, the same packing frustration that is giving rise to slow dynamics also appears to ultimately promote the formation of an ordered solid phase. This argues that the effect of confinement on the phase diagram of the system can provide important insights into how confinement impacts single-particle dynamics. The consequences of this could be significant for the strategies that are typically employed to study supercooled and confined liquids. For example, weak polydispersity is commonly incorporated into model fluid systems in order to study them under conditions where the corresponding monatomic fluid would rapidly crystallize. A cautionary note that follows from the above discussion is that one should not readily assume that the behaviors of the polydisperse and monatomic systems are trivially related, and that the former only differs from the latter, in that its liquid state is kinetically accessible over a broader range of conditions. The phase diagrams of polydisperse materials are considerably more complex than monatomic systems (even in the bulk.<sup>32</sup>) Thus, one should expect confinement to impact

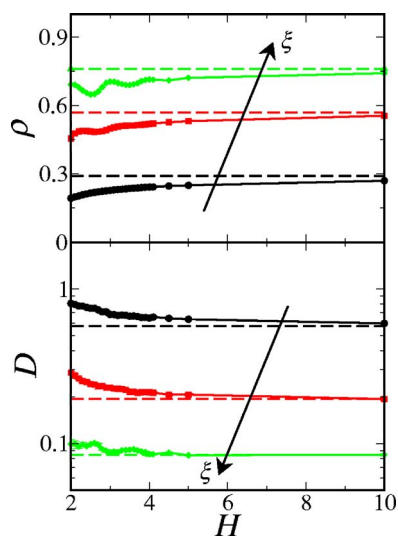


FIG. 6. (Color online) Average density  $\rho$  and self-diffusivity  $D$  as a function of pore size  $H$  for the confined HS fluid in equilibrium with the bulk HS fluid at a given activity  $\xi$  [ $\ln \xi=0.4, 4.4,$  and  $8.8$ ]. Dashed lines correspond to the density  $\rho_b$  and self-diffusivity  $D$  of the bulk HS fluid at the given activity  $\xi$ .

the dynamics of polydisperse systems in ways that are not easily relatable to the behavior of the corresponding monatomic fluids.

We now turn our attention to the  $H$ -dependent diffusivity behavior of the confined HS fluid at fixed activity  $\xi$  (i.e., in chemical equilibrium with the bulk). As can be ascertained from the strong correspondence between  $D$  and  $\rho$  in Fig. 4, the dynamical behavior at constant  $\xi$  can be largely predicted in advance if one simply has knowledge of how  $H$  influences  $\rho$  at constant  $\xi$  [e.g., from simulation or the analytical model of Eqs. (10) and (11)]. In Fig. 6, we provide the  $H$ -dependent data along constant  $\xi$  paths for the quantities  $\rho$  and  $D$  determined from GC-TMMC and DMD simulations, respectively. One initial observation is that  $\rho$  is always less than  $\rho_b$  for finite  $H$ , and, as should be expected based on this,  $D$  is larger in the pores than in the equilibrium bulk fluid. Note that this type of physically intuitive connection between average density and dynamics would be completely lost, however, if one instead chooses  $\rho_h$  as the definition for average density, which is significantly greater than  $\rho_b$  for finite  $H$ . More generally, the reliability of approximate theories for transport properties in inhomogeneous fluids could be particularly sensitive to how averaging is handled, which might help to explain why an earlier kinetic theory<sup>13</sup> predicts that confining a fluid at constant  $\xi$  significantly decreases  $D$ , the opposite of what is seen in the MD simulation data of Fig. 6.

A second observation about the data in Fig. 6 is that there are negative oscillatory deviations in  $\rho$  (relative to bulk) with  $H$  at high  $\xi$  in small pores, which one might expect to produce similar positive oscillations in  $D$ . However, the frustration-induced negative deviations from bulk behavior in the  $D$  vs  $H$  relationship at constant  $\rho$  shown in Fig. 4 appear to largely cancel this effect. The net result is that  $D$  is strikingly similar to bulk behavior, even for small  $H$ , along paths of constant (and sufficiently high)  $\xi$ .

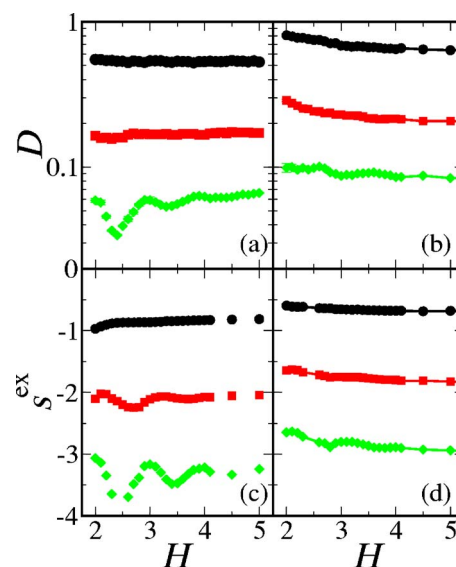


FIG. 7. (Color online) (a) Self-diffusivity  $D$  and (b) excess entropy  $s^{\text{ex}}$  as a function of pore size  $H$  for the confined HS fluid at a given pore packing fraction  $\phi=\pi\rho/6$ . Data from top to bottom correspond to  $\phi=0.15, 0.3,$  and  $0.4$ . (c) Self-diffusivity  $D$  and (d) excess entropy  $s^{\text{ex}}$  as a function of pore size  $H$  for the confined HS fluid at a given activity  $\xi$ . Data from top to bottom correspond to  $\ln \xi=0.4, 4.4,$  and  $8.8$ .

#### D. Diffusivity and excess entropy

The oscillatory data in Fig. 4 clearly show that average density alone cannot predict the self-diffusivity of the HS fluid if the fluid is both dense and confined to a pore smaller than approximately three diameters. Is there another thermodynamic quantity that can predict diffusivity behavior in these narrow pores? One promising candidate is the excess entropy  $s^{\text{ex}}$  (relative to ideal gas), which recent DMD simulations<sup>7</sup> demonstrate, to an excellent approximation, determines the self-diffusivity of the HS fluid confined between hard walls for  $H>3.5$ . Here, we explore its relationship to self-diffusivity in smaller pores.

Figure 7 shows the data for  $D$  and  $s^{\text{ex}}$  of the confined fluid collected from our DMD and GC-TMMC simulations [data at fixed pore packing fraction  $\phi$  provided in panels (a) and (c), and data at fixed activity  $\xi$  provided in (b) and (d)]. Irrespective of the thermodynamic path, strong qualitative correspondence is observed between  $D$  and  $s^{\text{ex}}$ , including the “in-phase” oscillations that emerge at small  $H$ . In other words, self-diffusivity and excess entropy appear to be affected in a very similar way by confinement, even for the very narrow pores.

To scrutinize the quantitative accuracy of the relation between the two variables, we also plot all data corresponding to constant pore packing fraction  $\phi$  (filled symbols) and constant  $\xi$  (empty symbols) paths in Fig. 8 in the  $D$ - $s^{\text{ex}}$  plane. As can be seen, most of the data fall very close to the curve for the bulk HS fluid, indicating that excess entropy (a static quantity) can indeed approximately predict the implications of confinement for self-diffusivity. The largest deviations are for the fluid that has the highest pore packing fraction of  $\phi=0.4$ .

These data are yet one more manifestation of a larger trend seen throughout this paper. Namely, that the confined

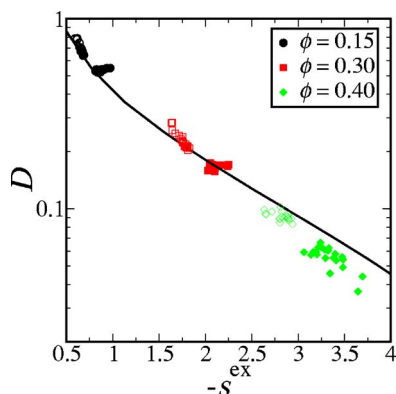


FIG. 8. (Color online) Self-diffusivity  $D$  vs negative excess entropy per particle  $-s^{\text{ex}}$  for the bulk HS fluid (solid curve) and for the HS fluid confined between smooth hard walls (symbols). The filled symbols correspond to the confined system at a fixed pore packing fraction  $\phi$  as shown on the legend, and empty symbols are for system at a given activity  $\xi$  for which bulk packing fraction is given on the legend.

HS fluid, by measure of many of its average properties, has behavior very similar to that of the bulk fluid. It changes character only under a fairly restrictive set of conditions, when the pore fluid is dense ( $\phi \geq 0.4$ ) and when it is confined to pores smaller than approximately three particle diameters in width.

#### IV. CONCLUSIONS

In conclusion, we have presented new comprehensive simulation results for the HS fluid confined between smooth hard walls. The results elucidate thermodynamic and dynamic behavior of this system over a wide range of system conditions, further clarifying the precise role of confinement on average fluid properties and the most useful way to define average density for this system. One perhaps unexpected result is that, for most conditions, the average behavior of the confined HS fluid is very similar to that of the bulk fluid. Frustration-induced finite effects do emerge in this system, but they are only prominent for very small pores (dimensions smaller than approximately three particle diameters) and high fluid densities where the system approaches the confinement-shifted fluid-solid phase boundary.

#### ACKNOWLEDGMENTS

One of the authors (J.M.) acknowledges the financial support from a Continuing University Fellowship of The University of Texas at Austin. Two of the authors (T.M.T. and J.R.E.) acknowledge the financial support of the Na-

tional Science Foundation under Grant Nos. CTS-0448721 and CTS-028772, respectively, and the Donors of the American Chemical Society Petroleum Research Fund under Grant Nos. 41432-G5 and 43452-AC5, respectively. The author (T.M.T.) also acknowledges the support of the David and Lucile Packard Foundation and the Alfred P. Sloan Foundation. The Texas Advanced Computing Center (TACC) and University at Buffalo Center for Computational Research provided computational resources for this study.

<sup>1</sup>H. T. Davis, *Statistical Mechanics of Phases, Interfaces, and Thin Films* (VCH, New York, 1996).

<sup>2</sup>A. Fortini and M. Dijkstra, *J. Phys.: Condens. Matter* **18**, L371 (2006).

<sup>3</sup>P. A. Thompson, G. S. Grest, and M. O. Robbins, *Phys. Rev. Lett.* **68**, 3448 (1992).

<sup>4</sup>M. Schmidt and H. Löwen, *Phys. Rev. Lett.* **76**, 4552 (1996).

<sup>5</sup>R. Zangi and S. A. Rice, *Phys. Rev. E* **58**, 7529 (1998).

<sup>6</sup>M. Schmidt and H. Löwen, *Phys. Rev. E* **55**, 7228 (1997).

<sup>7</sup>J. Mittal, J. R. Errington, and T. M. Truskett, *Phys. Rev. Lett.* **96**, 177804 (2006).

<sup>8</sup>M. Dijkstra, *Phys. Rev. Lett.* **93**, 108303 (2004).

<sup>9</sup>S. Auer and D. Frenkel, *Phys. Rev. Lett.* **91**, 015703 (2003).

<sup>10</sup>W. K. Kegel, *J. Chem. Phys.* **115**, 6538 (2001).

<sup>11</sup>M. Heni and H. Löwen, *Phys. Rev. E* **60**, 7057 (1999).

<sup>12</sup>J. J. Magda, M. V. Tirrell, and H. T. Davis, *J. Chem. Phys.* **83**, 1888 (1985).

<sup>13</sup>T. K. Vanderlick and H. T. Davis, *J. Chem. Phys.* **87**, 1791 (1987).

<sup>14</sup>J. R. Errington, *J. Chem. Phys.* **118**, 9915 (2003).

<sup>15</sup>J. R. Errington, *Phys. Rev. E* **67**, 012102 (2003).

<sup>16</sup>D. C. Rapaport, *The Art of Molecular Dynamics Simulation*, 2nd ed. (Cambridge University Press, Cambridge 2004).

<sup>17</sup>The activity is defined as  $\xi = \exp(\beta\mu)/\Lambda^3$ , where  $\mu$  is the chemical potential and  $\Lambda$  is the de Broglie wavelength.

<sup>18</sup>A. M. Ferrenberg and R. H. Swendsen, *Phys. Rev. Lett.* **61**, 2635 (1988).

<sup>19</sup>A. Z. Panagiotopoulos, *J. Phys.: Condens. Matter* **12**, R25 (2000).

<sup>20</sup>J. R. Errington and V. K. Shen, *J. Chem. Phys.* **123**, 164103 (2005).

<sup>21</sup>J. R. Henderson and F. van Swol, *Mol. Phys.* **51**, 991 (1984).

<sup>22</sup>I. Z. Fisher, *Statistical Theory of Liquids* (The University of Chicago Press, Chicago 1964).

<sup>23</sup>J. R. Errington, T. M. Truskett, and J. Mittal, *J. Chem. Phys.* **125**, 244502 (2006).

<sup>24</sup>N. F. Carnahan and K. E. Starling, *J. Chem. Phys.* **51**, 635 (1969).

<sup>25</sup>J. R. Henderson, *J. Chem. Phys.* **116**, 5039 (2002).

<sup>26</sup>P. Bryk, R. Roth, K. R. Mecke, and S. Dietrich, *Phys. Rev. E* **68**, 031602 (2003).

<sup>27</sup>D. Henderson and M. Plischke, *Proc. R. Soc. London, Ser. A* **400**, 163 (1985).

<sup>28</sup>S. Torquato, T. M. Truskett, and P. G. Debenedetti, *Phys. Rev. Lett.* **84**, 2064 (2000).

<sup>29</sup>T. M. Truskett, S. Torquato, and P. G. Debenedetti, *Phys. Rev. E* **62**, 993 (2000).

<sup>30</sup>R. Kjellander and S. Sarman, *J. Chem. Soc., Faraday Trans.* **87**, 1869 (1991).

<sup>31</sup>M. Alcoutlabi and G. B. McKenna, *J. Phys.: Condens. Matter* **17**, R461 (2005).

<sup>32</sup>P. Sollich, *J. Phys.: Condens. Matter* **14**, R79 (2002).